# Defect ordering in aliovalently doped cubic zirconia from first principles

A. Bogicevic, C. Wolverton, G. M. Crosbie, and E. B. Stechel
*Scientific Research Laboratories, Ford Motor Company, Dearborn, Michigan 48121-2053*
(Received 31 January 2001; published 13 June 2001)

Defect ordering in aliovalently doped cubic-stabilized zirconia is studied using gradient corrected density-functional calculations. Intra- and intersublattice ordering interactions are investigated for both cation (Zr and dopant ions) and anion (oxygen ions and vacancies) species. For yttria-stabilized zirconia, the crystal structure of the experimentally identified, ordered compound $\delta$-$Zr_3Y_4O_{12}$ is established, and we predict metastable zirconia-rich ordered phases. Anion vacancies repel each other at short separations, but show an energetic tendency to align as third-nearest neighbors along $\langle 111 \rangle$ directions. Calculations with divalent (Be, Mg, Ca, Sr, Ba) and trivalent (Y, Sc, B, Al, Ga, In) oxides show that anion vacancies prefer to be close to the smaller of the cations (Zr or dopant ion). When the dopant cation is close in size to Zr, the vacancies show no particular preference, and are thus less prone to be bound preferentially to any particular cation type when the vacancies traverse such oxides. This ordering tendency offers insight into the observed high conductivity of $Y_2O_3$- and $Sc_2O_3$-stabilized zirconia, as well as recent results using, e.g., lanthanide oxides. The calculations point to $In_2O_3$ as a particularly promising stabilizer for high ionic conductivity. Thus we are able to directly link (thermodynamic) defect ordering to (kinetic) ionic conductivity in cubic-stabilized zirconia using first-principles atomistic calculations.

DOI: 10.1103/PhysRevB.64.014106 PACS number(s): 64.60.Cn, 81.30.Dz, 61.18.−j, 71.15.Mb

## I. INTRODUCTION

Despite decades of extensive use of zirconia ceramics in many technological applications, this surprisingly complex material still continues to exhibit remarkable properties that have yet to be explained by simple physical models. When pure zirconia, $ZrO_2$, is alloyed with other oxides, the high-temperature cubic polymorph can be stabilized to low temperatures, where its mechanical, thermal, and electrical properties are utilized in a large number of technological applications. One of the most prominent characteristics of this cubic fluorite phase is its high ionic conductivity, discovered by Nernst a century ago,[1] and subsequently explained by Wagner[2] to arise from charge compensating oxygen vacancies associated with aliovalent cation additions. Because its substantial band gap inhibits electronic conduction, cubic-stabilized zirconia has found widespread use as electrolyte membranes in solid oxide fuel cells, oxygen pumps and separators, and other electrochemical devices.[3–5]

Although the number of vacancies increases monotonically with dopant concentration,[6] measurements of the ionic conductivity in doped zirconia always exhibit a maximum for some critical dopant composition, with significantly decreased conductivity for lower and higher dopant levels.[5] Several attempts have been made to explain this nonmonotonic behavior of the conductivity in doped zirconias in terms of ordering and clustering tendencies between vacancies, oxygen ions, and dopant ions[7,8] or alternative physical models.[9] Additionally, for low levels of yttria, the cubic phase can give way to two-phase equilibria with the other two zero-pressure zirconia polymorphs, the tetragonal and monoclinic phases, which substantially affects the ionic conductivity. Given the conflicting accounts in the literature, the explanation of conductivity versus composition and temperature still remains largely unanswered. For instance, considering just a single dopant oxide (yttria), there are many contradictory experimental reports of whether the oxygen vacancies prefer to bind next to dopant ($Y^{3+}$) (Refs. 10–15) or host ($Zr^{4+}$) cations.[16–20] In addition, it is well established that defect ordering and clustering directly contribute to the observed conductivity degradation upon aging of electrolytes.[3,21] Hence, a more complete picture of the ordering tendencies in cubic stabilized zirconias is needed to facilitate a generic understanding of the ionic conductivity in these materials.

The stabilized cubic phase of $ZrO_2$ poses an interesting, multifaceted ordering problem. The fluorite structure consists of two sublattices: an fcc cation sublattice, consisting of Zr and dopant ions, and a simple cubic anion sublattice, consisting of oxygen ions and oxygen vacancies (denoted $\square$), the latter being introduced to compensate for the charge associated with nonisovalent doping on the cation lattice. This dual sublattice geometry leads to three distinct forms of intra- and intersublattice interactions: (i) The *cation-cation* or Zr-dopant interaction on the cation sublattice, (ii) the *anion-anion* or oxygen-$\square$ interaction on the anion sublattice, and (iii) the *cation-anion* or dopant-$\square$ interaction between the two sublattices. Each of these three interactions may be either of ''ordering type'' (association of unlike species, e.g., O and $\square$) or ''clustering type'' (association of like species), and depends on the separation shell (i.e., nearest neighbor, next nearest neighbor, etc.). Additionally, the three interactions are not necessarily independent, and so the ordering tendencies may be (and most often are) coupled. These considerations underscore the complexity inherent in this seemingly simple system.

In this paper, we report on an extensive first-principles study of the currently most common and versatile solid-state electrolyte, yttria-stabilized zirconia (YSZ). An in-depth analysis of defect ordering at selected compositions reveals the energetically preferred ordering tendencies between cation ($Y^{3+}$, $Zr^{4+}$) and anion ($O^{2-}$, $\square$) species. Anion vacan-

 

cies are found to prefer Zr coordination, and vacancy-vacancy pairs align (or ''cluster'') as third nearest neighbors along $\langle 111 \rangle$ directions. We also find a large energy dependence on the cation (Zr/Y) configuration, which is quite interesting considering that cation-cation ordering has been almost completely ignored in the literature. Our calculations establish the complete crystal structure of the only experimentally identified ordered compound, $\delta$-$Zr_3Y_4O_{12}$, and reveal the existence of new low-energy metastable zirconia-rich ordered phases. In addition, a series of zirconia calculations for other additive systems demonstrates that in stabilizing with divalent (Be, Mg, Ca, Sr, Ba) and trivalent (Y, Sc, B, Al, Ga, In) oxides, anion vacancies in general prefer to be close to the smaller of the two cations (either Zr or the dopant ion). With dopant ions similar in size to $Zr^{4+}$, vacancies show little preference, and are thus less likely to be bound to any specific cation site as the vacancies traverse the material. These results offer insight into the high conductivity of $Y_2O_3$- and $Sc_2O_3$-stabilized zirconia, and highlight $In_2O_3$ as a promising dopant candidate for high ionic conductivity in stabilized zirconias.

The organization of the paper is as follows: Sec. II describes our theoretical first-principles approach, Sec. III reports our results for the constituent divalent, trivalent, and tetravalent oxides. Section IV presents an extensive study of yttria stabilized zirconia, including a detailed analysis of defect interactions and ordered compounds. Section V contains our results and analysis for divalent- and trivalent-cation stabilized zirconias, and Sec. VI formulates our conclusions. Finally, the Appendix displays some of the more technical results.

## II. METHODOLOGY

The basis for the electronic-structure calculations is density-functional theory (DFT),[22,23] with core-electron interactions described by ultrasoft Vanderbilt pseudopotentials,[24] as implemented in the highly efficient VASP code.[25] We expand the one-electron wave functions in a plane-wave basis with an energy cutoff of 29 Ry, keeping semicore electrons in the valence for all cations. For the exchange-correlation functional, we use the PW91 implementation of the generalized gradient approximation (GGA).[26] To facilitate comparisons with previous DFT calculations and to assess the significance of adding gradient corrections, we also perform a series of YSZ calculations using the Ceperley-Alder implementation of the local-density approximation (LDA),[27] both with and without semicore *p* electrons in the valence. The Appendix contains these results. We solve the Kohn-Sham equations iteratively, and optimize all atomic positions, cell shape, and cell volume using a conjugate gradient algorithm until residual atomic forces are less than 0.03 eV/Å. The Brillouin zone sampling[25] uses increasingly more dense Monkhorst-Pack **k**-point meshes, until acheiving *absolute* convergence (to $\leqslant 1$ meV). In most cases, a $(4\times4\times4)$ **k**-point mesh is sufficient, although some cases require up to $(7\times7\times7)$ sampling. For stabilizing oxides other than yttria, a smaller $(2\times2\times2)$ mesh was used, which reproduces absolutely converged formation enthalpies to within 10 meV. To enhance convergence with respect to Brillouin zone sampling, we employ a Fermi smearing of the electronic occupancy with a fictitious electronic temperature of 0.2 eV. In certain structures where the bandgap turns out to be substantially decreased, a smaller smearing width of 0.1 eV is used to reduce the electronic entropy below 1 meV/ion. All calculations use primitive unit cells, which in the case of the pure oxides means unit cells with from 2 (rocksalt structure) to 40 (bixbyite structure) atoms, and for the doped-zirconia cells considered here, 11–23 atoms.

## III. PURE OXIDES

Pure zirconia exhibits three zero-pressure phases. The low-temperature monoclinic phase is stable up to about 1400 K, at which temperature it transforms into a tetragonal structure. At about 2650 K, this phase converts into the cubic fluorite structure, which is stable up to the melting point of zirconia (about 2990 K).[20] Several studies of these three stable $ZrO_2$ phases have been reported previously using first-principles methods.[28–36] Although some of the early accounts failed to reproduce the correct energetic ordering of the three zero-pressure polymorphs, the most recent reports do not have this problem, and are quantitatively in good mutual agreement.[29,32,34] Since our LDA calculations for all zirconia polymorphs are in excellent agreement with many of these previous reports, we relegate the results for these phases to the Appendix. We emphasize here that the present calculations are based on minimal radii ultrasoft pseudopotentials, keeping semicore states in the valence, and correctly reproduce the experimental hierarchy of pure zirconia structures: $E^{\mathrm{m}}_{\mathrm{ZrO_2}} < E^{\mathrm{t}}_{\mathrm{ZrO_2}} < E^{\mathrm{c}}_{\mathrm{ZrO_2}}$, where the superscripts identify the three phases by their first letters.

Among the trivalent pure oxides, those with intermediately sized cations ($Y_2O_3$, $Sc_2O_3$, $In_2O_3$) all assume the bixbyite structure at low temperatures, while oxides with smaller cations order into corundum ($Al_2O_3$) and other sesquioxide structures ($B_2O_3$, $Ga_2O_3$).[37] Regarding divalent additives, the simple rocksalt structure is prevalent in oxides with intermediate-sized cations (MgO, CaO, SrO, BaO), while the oxide with the smallest cation (BeO) assumes a zincite structure.[37,38] The computed (GGA) and experimental structure parameters for these oxides are summarized in Table I, while some of the details are left for the Appendix. Overall, these results agree quite well with experiment, albeit with the customary small but systematic GGA overestimate of experimentally established lattice parameters.

## IV. YTTRIA-STABILIZED ZIRCONIA

The addition of even minute amounts of yttria strongly affects the structural integrity of the pure zirconia phases. As aliovalent cations are substituted for Zr ions, vacancies are created on the anion lattice to maintain charge neutrality. In the case of YSZ, one oxygen ion is removed for every unit of $Y_2O_3$ introduced into the zirconia. The most palpable crystallographic effect upon aliovalent doping is the rapid stabilization of the tetragonal and cubic phases towards lower

TABLE I. Experimental and calculated (GGA) structural parameters of pure oxides. The experimental values are reported extrapolations to 0 K The lattice constants are all given in Å, while $\alpha/\beta$ denotes the rhombohedral ($\alpha$) or monoclinic ($\beta$) angle in degrees. The superscript in the case of zirconia denotes the cubic, tetragonal, and monoclinic phases of $ZrO_2$ (see text). The experimental (room-temperature) results are taken from Ref. 37, except those for $ZrO_2$ which are taken from Ref. 39.

| | $a_0$ (Å) | | $b_0$ (Å) | | $c_0$ (Å) | | $\alpha/\beta$ | |
|---|---|---|---|---|---|---|---|---|
| | Expt. | GGA | Expt. | GGA | Expt. | GGA | Expt. | GGA |
| $ZrO_2^c$ | 5.08 | 5.16 | | | | | | |
| $ZrO_2^t$ | 3.60 | 3.65 | | | 5.18 | 5.30 | | |
| $ZrO_2^m$ | 5.15 | 5.23 | 5.21 | 5.30 | 5.32 | 5.41 | 99.2° | 99.6° |
| $Y_2O_3$ | 10.60 | 10.77 | | | | | | |
| $Sc_2O_3$ | 9.85 | 9.99 | | | | | | |
| $B_2O_3$ | 4.33 | 4.40 | | | | | | |
| $Al_2O_3$ | 5.13 | 5.16 | | | | | 55.3° | 55.3° |
| $Ga_2O_3$ | 5.32 | 5.39 | | | | | 55.8° | 55.8° |
| $In_2O_3$ | 10.12 | 10.38 | | | | | | |
| BeO | 2.70 | 2.71 | | | 4.38 | 4.40 | | |
| MgO | 4.21 | 4.26 | | | | | | |
| CaO | 4.81 | 4.82 | | | | | | |
| SrO | 5.16 | 5.18 | | | | | | |
| BaO | 5.52 | 5.68 | | | | | | |

temperatures when the dopant content is increased, as illustrated schematically in the $Y_2O_3$-$ZrO_2$ phase diagram of Fig. 1, redrawn from Ref. 40.

The mechanism behind the stabilization of the high-temperature zirconia polymorphs has been the subject of some controversy.[34,41–43] The prevailing explanation is based on observations that increasing covalency favors structures

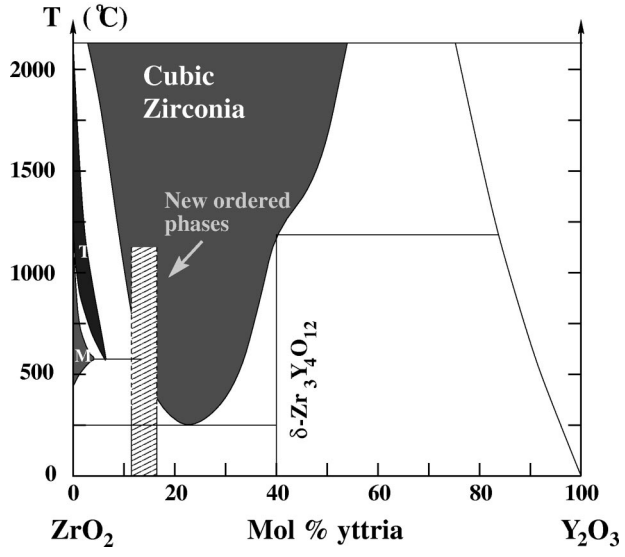


FIG. 1. Schematic illustration of the $Y_2O_3$-$ZrO_2$ composition-temperature phase diagram, redrawn from Ref. 40. The monoclinic and tetragonal phases are indicated by their first letter. Compositions where new ordered (meta)stable phases have been found are highlighted schematically.

with lower coordination (see Ref. 41 for an extensive discussion on this topic). Based on this argument, it has been suggested that the stabilization of the cubic phase arises from the tendency for the Zr ions to assume the sevenfold anion coordination of the lowest-energy monoclinic phase.[34,41] Since cubic zirconia only offers eightfold-coordinated cation sites, this lowering of the $Zr^{4+}$ ion coordination is presumably enabled by the oxygen vacancies introduced upon the aliovalent doping. Note that this model implicitly demands that vacancies closely associate with the Zr ions rather than dopant ions ($Y^{3+}$ in the case of YSZ), making strong predictions for anion-cation defect ordering in YSZ. In addition, this coordination-driven argument implies that the qualitative features of the anion-cation defect ordering should be independent of the type of (trivalent) dopant used.

While this coordination-driven argument certainly has some intuitive appeal, it is based on simple empirical observations and remains as of yet unproven. Obviously, the stabilization mechanism depends critically on how the vacancies are distributed within the doped zirconia, and as we will demonstrate, this ordering can be quite counterintuitive. Since the vacancies are also what provides the high ionic conductivity of cubic stabilized zirconia by facilitating diffusion of oxygen ions, an understanding of defect ordering in this material cuts straight to the very essence of its ionic conductivity.

### A. Structures and energetics

As explained above, a complete description of the available configuration space for cubic-stabilized zirconias must include ordering and clustering tendencies on both cation and anion sublattices, as well as the interaction between the two sublattices. As the doped zirconia systems are much more complex than the pure zirconia phases, the majority of the computational work on these systems has been based on (semi)empirical approaches.[44–47] The recent studies by Gennard *et al.*[33] and Stapper *et al.*[34] are, to our knowledge, the only existing first principles study of yttria-stabilized zirconia. In the following, we describe our study of these three ordering tendencies via the energetic dependence of the total cation and anion configuration, as calculated from first principles. To this end, we investigate 90 different hypothetical cation and anion ordered arrangements at several different dopant compositions (described below). Although our calculations are for zero temperature (i.e., no entropic effects are included), they allow us to uncover the generic ordering tendencies that exist in this system.

By combining $ZrO_2$ and $Y_2O_3$ with mole fractions $1-x$ and $x$, respectively, one obtains a YSZ stoichiometry given by $Zr_{1-x}Y_{2x}O_{2+x}$. The energetics of this YSZ compound can be expressed in terms of its formation enthalpy (with respect to cubic $ZrO_2$),

$$\Delta H = E[Zr_{1-x}Y_{2x}O_{2+x}] - [(1-x)E(ZrO_2^c) + xE(Y_2O_3)], \quad (1)$$

the (zero-pressure) energy difference between the YSZ compound and the composition-weighted average of its constituent oxides. A negative formation enthalpy indicates the sta-

bility of the compound relative to phase separation into the constituent oxides, whereas a positive formation enthalpy indicates that phase separation is preferred in the absence of entropic effects.

#### *1. Identification of the δ-$Zr_3Y_4O_{12}$ crystal structure*

In the observed $Y_2O_3$-$ZrO_3$ phase diagram (Fig. 1), there exists only one intermediate ordered compound, $\delta$-$Zr_3Y_4O_{12}$. The long-range ordering of this phase is often assumed to be correlated with the short-range ordering of the solid solution phase, and therefore connected with the ionic conductivity of YSZ. The $\delta$ phase is generally acknowledged to be based on the fluorite lattice, with ordering of the charge compensating vacancies along $\langle 111 \rangle$ directions. Although the cell vectors and anion ordering have been established in neutron scattering[20,40,48,49] and other scattering experiments, the complete cation ordering has so far eluded experimental identification due to the weak scattering contrast between Y and Zr ions and the possibility of cation disorder in the structure at high temperatures.

In order to improve this situation, we have undertaken an investigation of the $\delta$-$Zr_3Y_4O_{12}$ phase using first-principles total-energy calculations, searching for the lowest-energy ion configuration(s) without any *a priori* assumptions of the ordering on any of the sublattices. The only input to these calculations are two pieces of experimental information: (i) the observed cell vectors and (ii) the observation that this structure is fluorite based. One might imagine that with this limited set of information, the number of possible configurations would be too large to sample efficiently with computationally demanding electronic-structure methods. However, with the aid of advanced lattice algebra techniques developed for Ising-model studies of alloys, we demonstrate that one can *completely* search the allowed configuration space and find the ''winning'' (minimum energy) configuration corresponding to $\delta$-$Zr_3Y_4O_{12}$.

The observed cell vectors are rhombohedral, and the primitive cell contains one (fluorite-based) formula unit, or seven cations. Because the experimentally refined cation positions include some fractionally occupied sites, we cannot rule out the possibility that the true $Zr_3Y_4O_{12}$ ground state at this composition contains more than one formula unit in the primitive cell. In what follows, we assume a primitive cell of one formula unit (in accord with the observed cell vectors), and determine the energy-minimizing ion positions within this cell.

The cation positions in the fluorite structure fall on an fcc lattice. Lattice algebra techniques have been devised[50] to enumerate the total number of possible binary fcc-based configurations for a specified number of sites. Using these methodologies, we find that for a seven-atom fcc cell, there are 104 possible configurations, each with a large number of ordering possibilities on the anion lattice. However, only two of these distinct cation configurations possess rhombohedral cell vectors. For each of these two seven-cation configurations, 14 anions were placed in the fluorite positions, and a symmetry analysis was performed to determine which of the anion positions were symmetrically inequivalent. Armed with this knowledge, we then specify all of the symmetry-distinct ways to remove the two vacancies from this structure to yield the stoichiometry $Zr_3Y_4O_{12}$ (with a total of 19 atoms per unit-cell). There are 45 such possible configurations, and we have calculated the total energies (absolutely converged with respect to Brillouin zone sampling), and fully relaxed geometries for each of these 45 (19-atom) configurations from first principles. We note that an analogous approach to the one outlined above has recently been used to successfully elucidate from first principles the structure of another complex oxide phase, $\kappa$-$Al_2O_3$.[51]

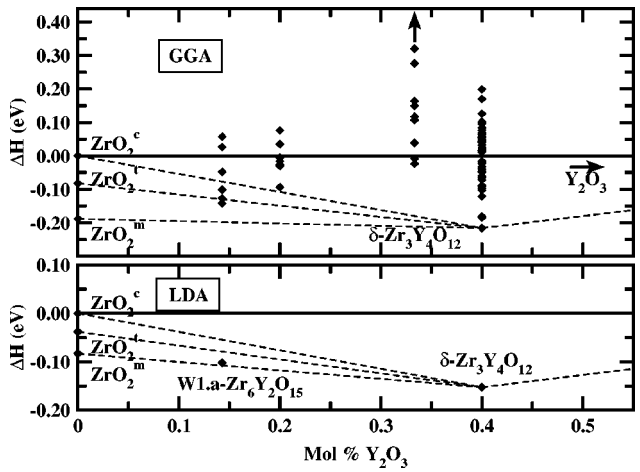


FIG. 2. Formation enthalpies (eV/$Zr_{1-x}Y_{2x}O_{2+x}$ formula unit) for an ensemble of symmetrically inequivalent YSZ structures at four different compositions, as computed within DFT-GGA and DFT-LDA.

The calculated formation enthalpies for the 45 YSZ structures are shown in Fig. 2. Roughly half have a negative formation enthalpy, and the one structure with the lowest $\Delta H$ we identify as the experimentally observed $\delta$ phase. We give the complete crystal structure of this DFT-deduced $\delta$ phase in the Appendix. Despite the fact that no experimental information on the cell internal ordering was used to find this structure, the predicted low-energy phase contains vacancies which are aligned along $\langle 111 \rangle$ directions, in agreement with experimental refinements of the $\delta$ phase.[20] In addition, we find that the only sixfold coordinated cation site in the $\delta$ phase is occupied by a Zr ion, as measured in scattering experiments of YSZ (Ref. 40) and other stabilized zirconia systems.[52,53] Thus, we consider that our assumption of one formula unit per primitive cell is reasonable. Vacancy and dopant ordering preferences among these 45 structures, as well as other structures with different compositions, are discussed in detail below.

#### *2. ''Artificial'' cation superlattices*

Although the $\delta$-$Zr_3Y_4O_{12}$ phase provides some understanding of the ordering tendencies in YSZ, this particular compound has a higher yttria content than typically used in zirconia-based electrolyte applications. For this reason, we focus our study on the zirconia-rich part of the YSZ phase diagram, where we investigate the energetics and ordering at

several compositions more Zr rich than $Zr_3Y_4O_{12}$. The complete range of compositions studied (with the mole fractions of yttria, $x$) is

$$Zr_3Y_4O_{12} \quad (x=0.40),$$

$$Zr_2Y_2O_7 \quad (x=0.33),$$

$$Zr_4Y_2O_{11} \quad (x=0.20),$$

$$Zr_6Y_2O_{15} \quad (x=0.14).$$

Although no ordered phases have been observed[54] in YSZ for $x=0.33$, 0.20, or 0.14, we chose to study these compositions as they allow for relatively simple and systematic characterization of the ionic configurations: Using the same lattice algebra techniques as described above, we can enumerate all of the possible cell shapes and configurations for fluorite-based structures with two, three, and four cations per cell. For Zr-rich compositions, these cells possess cation stoichiometries of ZrY (two cations), $Zr_2Y$ (three cations), $Zr_3Y$ (four cations), or $Zr_2Y_2$ (four cations). Because charge conservation in YSZ requires half as many vacancies as dopant Y ions, the ZrY, $Zr_2Y$, and $Zr_3Y$ cation cells have to be doubled in order to yield an integer number of vacancies. Many of these configurations correspond to a superlattice stacking of cations along $\langle 100\rangle$, $\langle 111\rangle$, $\langle 110\rangle$, $\langle 201\rangle$, and $\langle 311\rangle$. We note that each of these structures (unlike the $Zr_3Y_4O_{12}$ structures described above) contains only two $Y^{3+}$ ions and, hence, only one vacancy. For each cation configuration, a symmetry analysis of the anion positions was performed to determine all of the distinct possible placements of the oxygen vacancy. These artificial Zr/Y superlattices, when added to the 45 $Zr_3Y_4O_{12}$ structures above, yield a total of 90 structures considered here to sample the configuration space of YSZ. For each of these structures, we compute the enthalpies of formation with respect to the pure zirconia and yttria according to Eq. (1). The computed formation enthalpies for all 90 structures are displayed in Fig. 2 (some of the highest energy $Zr_2Y_2O_7$ structures fall outside the graph, as indicated by the vertical arrow). Below we first make some general observations and then proceed in a systematic way to analyze the results in terms of the various energetically preferred defect interactions in this system.

The large scatter in formation enthalpies among structures with the same composition but different defect ordering gives a first indication of how sensitive the energetics are to the relative positions of the defects. In particular, the structures with the stoichiometry $Zr_2Y_2O_7$ (which includes the pyrochlore structure) display a wide range of formation enthalpies, but they are almost all positive, i.e., unstable with respect to phase separation. The high energy of the $Zr_2Y_2O_7$ structures is consistent with the fact that such ordered structures have eluded observation, and an early report of the existence of a pyrochlore structure in this system is likely spurious.[54]

#### *3. Ordered ground states*

In a plot of energy versus composition, such as Fig. 2, it is reasonable to ask what the stable (low-temperature) ''ground states'' are. For a given ordered compound to be a ground state, it must satisfy both of the following criteria: (a) a ground state must be lower in energy than any other structure at the particular composition and (b) a ground state must be lower in energy than any two-phase mixture of structures at other compositions. A particular example of the latter criterion is that a structure must be lower in energy than a mixture of the constituents or $\Delta H<0$ [Eq. (1)]. Following these criteria, one may find the ground states by a ''convex hull'' construction where tie lines are drawn between all low-energy phases, and only the minimum-energy tie lines are retained. These segments must necessarily be convex upward, since any concave downward region would indicate an instability towards phase separation between two neighboring phases.

Given that no other ordered compounds but the $\delta$ phase have been experimentally observed in YSZ, one would expect the low-temperature ground states of this system to consist solely of $ZrO_2^m$, $\delta$-$Zr_3Y_4O_{12}$, and $Y_2O_3$. As expected, we find these three phases on the convex hull within both the GGA and LDA (Fig. 2). Surprisingly, however, the energies of several of the $Zr_6Y_2O_{15}$ structures fall below the $ZrO_2^c + \delta$-$Zr_3Y_4O_{12}$ tie line, and one of them even falls below the $ZrO_2^t + \delta$-$Zr_3Y_4O_{12}$ tie line. This suggests new stable ordered structures with respect to cubic- and tetragonal-based YSZ, which, however, are metastable with respect to monoclinic YSZ (although within LDA one of the structures actually comes very close to the $ZrO_2^m + \delta$-$Zr_3Y_4O_{12}$ tie line). These low-energy structures correspond to $Zr_3Y$ superlattices along $\langle 311\rangle$, which we denote ''W1.'' Because the 90 structures we consider here are still a fairly limited sampling of the available configuration space for YSZ, the $Zr_6Y_2O_{15}$ low-energy phase must be viewed as an upper bound to the true energetics of zirconia-rich YSZ. Since we can happen upon one metastable compound at this composition from a very limited sampling of configurations, it is quite likely that there are even lower $\Delta H$ structures undetected. These lower-energy structures might very well fall below the $ZrO_2^m + \delta$-$Zr_3Y_4O_{12}$ tie line, and therefore in addition to the only observed ordered $\delta$ phase in the YSZ phase diagram, there must exist at least metastable and possibly stable zirconia-rich phases that are yet to be observed.

Whether or not new stable Zr-rich phases actually exist, their observation could be hampered at low temperatures, where it takes prohibitively long times to reach thermodynamic equilibrium due to exceedingly sluggish cation diffusion. It is imperative to realize at this point that these new zirconia-rich ordered phases are important not just at low temperatures, but also at elevated temperatures where the disordered solid solution is stable. The reason is that remnants of the low-temperature long-range order, even for metastable phases, are likely to survive as short-range order in the high-temperature solid solution phase, which in turn affects defect interactions and consequently ionic diffusion. This connection between long-range and short-range order-

ing tendencies is a very common occurence (as exemplified by the ⟨111⟩ ordering of vacancies in YSZ solid solution regimes where the $\delta$ phase is unstable), although exceptions have been noted in some metallic alloys. The classification of all of these long- versus short-range order types can be understood in terms of the energetics of the ordered, random, and phase-separated states of the system in question.[55]

### B. Defect interactions

We have already indicated that the defect interactions in yttria-stabilized zirconia can quantitatively affect formation enthalpies and even qualitatively decide the type of long-range ordering that will occur at low temperatures. Since both short-range ordering and long-range ordering are prone to decrease ion mobility, it is essential to have a good understanding of the various types of defect interactions that take place in YSZ. To this end, we have performed a detailed analysis of the vacancy-vacancy, vacancy-dopant, and dopant-dopant interactions in fluorite-based YSZ compounds, both in the observed $\delta$-$Zr_3Y_4O_{12}$ phase and the newly predicted zirconia-rich ordered compounds.

#### *1. Vacancy-vacancy interactions*

Compared with the nominal charges of the host $Zr^{4+}$ and $O^{2-}$ ions, the $Y^{3+}$ ions and anion vacancies can be viewed as point defects with charges $1-$ and $2+$, respectively. Thus, from simple point-charge electrostatics, one would expect the vacancies to repel each other. Diffuse neutron and x-ray scattering experiments[20,40,48,49] suggest that there is a strong tendency for anion vacancies to align along ⟨111⟩ directions in both the solid solution fluorite phase of zirconia, as well as the ordered $\delta$-$Zr_3Y_4O_{12}$ compound. Out of the four different YSZ compositions we consider here, only the structures with the $\delta$-phase composition offer a way to address this issue since there are two vacancies per unit cell of $Zr_3Y_4O_{12}$ (in the other compositions we study, there is only one vacancy per unit cell, and thus no way to isolate vacancy-vacancy interactions). To calculate vacancy-vacancy and vacancy-ion distances, it is necessary to first define the vacancy positions. For the perfect fluorite lattice, the vacancy positions are well defined, and for the relaxed cells, we simply take these ideal fluorite cell internal positions as the vacancy coordinates, which are admittedly ill defined due to asymmetric ionic relaxations. Figure 3 shows the computed formation enthalpies versus average vacancy-Zr distance for the 45 $Zr_3Y_4O_{12}$ structures. These 45 data points are categorized according to the smallest vacancy-vacancy distance (e.g., first, second, or third neighbor) and also with respect to the two cation ordering possibilities (labeled ''A'' and ''B''). With regard to the vacancy-vacancy ordering, we note that in Fig. 3 there is a strong correlation between the formation enthalpies and the mean vacancy separation: instances where the two vacancies are as far apart as possible (third nearest neighbors along ⟨111⟩ directions) are clearly the most favorable structures (i.e., have the lowest formation enthalpies), including the ground-state $\delta$ phase. Structures with nearest-neighboring vacancies (along ⟨100⟩) are all significantly higher in energy, and those

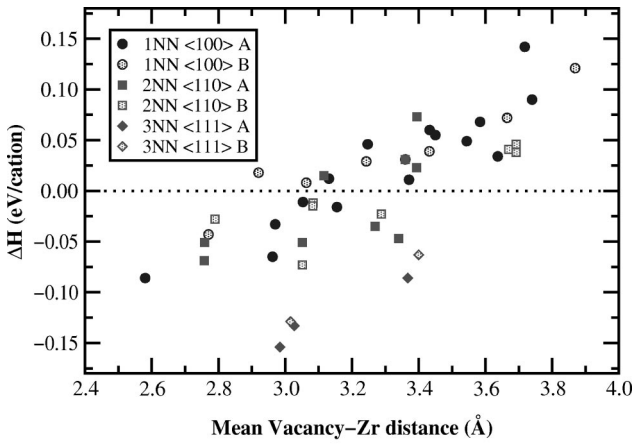


FIG. 3. Formation enthalpies (eV/cation) vs mean vacancy-zirconia separation for all 45 distinctly different $Zr_3Y_4O_{12}$ compounds as computed within DFT-GGA. The data are categorized according to the three possible vacancy-vacancy shells (1NN, 2NN, 3NN) and illustrate how the vacancies prefer being third nearest neighbors (in ⟨111⟩ directions) to each other and nearest neighbors to the host $Zr^{4+}$ ions. Within each vacancy-vacancy shell, the data are further separated into two subsets for each of the two distinct cation structural possibilities ''A'' and ''B.''

with next-nearest-neighboring vacancies (along ⟨110⟩) fall in between these two extremes. Thus, *our calculations demonstrate a vacancy-vacancy repulsion, consistent with both simple electrostatic considerations and experimental observations of vacancy clustering along* ⟨111⟩ *directions.*

Note that for the $Zr_3Y_4O_{12}$ stoichiometry, the amount of $Y^{3+}$ ions, and therefore the number of vacancies, is quite large (40 mol % $Y_2O_3$). Hence, the largest attainable (minimal) vacancy-vacancy separation for any of these structures is third nearest neighbors (3NN). For more dilute compositions, at the higher temperatures where the cubic phase remains, the vacancies could conceivably space themselves at distances greater than third neighbor. If the vacancy-vacancy ordering were driven purely by electrostatic considerations, one would expect that the vacancies would repel one another at all distances. Recent diffuse scattering measurements[20] of the cubic solid solution phase with ~10–24 mol % $Y_2O_3$ show vacancy pairs clustering along ⟨111⟩ as third nearest neighbors. Mechanical and dielectric loss measurements of single crystals[56] also support the ⟨111⟩ directionality of vacancy ordering. These measurements demonstrate that the defect ordering in YSZ is more complex than rendered by pure electrostatics, and as we show below, the vacancy-dopant ordering tendency competes with the electrostatic repulsion between vacancies.

#### *2. Vacancy-dopant interactions*

Simple electrostatics dictates that oppositely charged cation and anion defects should attract each other. For instance, Y ions and oxygen vacancies (with point charges $1-$ and $2+$ with respect to the host ions) should bind electrostatically. On the other hand, the lowest-energy monoclinic phase of pure zirconia contains seven fold-coordinated Zr ions, whereas the perfect fluorite phase only offers eightfold coor-

dination. This coordination-driven tendency would imply that vacancies should prefer to be closer to Zr ions so as to reduce the Zr coordination. Indeed, recent neutron scattering[20] and extended x-ray absorption fine structure (EXAFS) experiments,[16,19] as well as first-principles[34] and semi-empirical calculations,[44,45] all point to the association of vacancies with Zr rather than the Y ions, in clear disagreement with simple electrostatic considerations. However, as we show below, the coordination-based argument alone cannot explain the observed $Zr^{4+}$-□ ordering tendency.

We first note that our calculations fully corroborate previous findings of $Zr^{4+}$-□ association for all four compositions considered here. To illustrate this point, we once again refer the reader to the $Zr_3Y_4O_{12}$ results in Fig. 3. It is evident from this analysis that within each vacancy-vacancy coordination shell, there is a significant increase in the formation enthalpy (towards positive values) with the average vacancy-Zr separation. Identical trends are found for the other stoichiometries. Thus, *there is a clear driving force for the vacancies to closely associate with the Zr ions rather than the dopant ions, in contrast to simple electrostatic point-charge considerations*.

From our $Zr_3Y_4O_{12}$ results, as well as those of other more zirconia-rich compositions, we find that the most energetically favorable structures have a pair of vacancies associated with a single Zr cation. In this most favorable case, the central Zr ion is sixfold coordinated, demonstrating that the argument of the sevenfold coordination in monoclinic $ZrO_2$ cannot fully explain the $Zr^{4+}$-□ association. While this result is yet to be verified experimentally for YSZ, scattering studies with dopants other than yttria (yielding a higher Zr-dopant contrast) have shown that, whenever cation ordering is observable, it is always the smaller of the cations that assumes the sixfold coordination[52]—in excellent agreement with our calculations. Indeed, both experimental and recent model-potential studies have found that for many of the smaller dopant ions, vacancies in stabilized zirconia actually prefer to bind to dopants rather than host ions. We investigate this point from first principles below (see Sec. V).

For the sixfold-coordinated Zr cation, a competition ensues between the $Zr^{4+}$-□ ordering tendency and the □-□ repulsion. The repulsion between the pair of vacancies surrounding a single cation is minimized when the vacancies align as 3NN, along ⟨111⟩, providing an explanation for the results of the previous section, as well as the experimental findings of ⟨111⟩ vacancy pairs in dilute compositions, where the vacancies could conceivably be further apart than 3NN. Therefore, although the vacancy-vacancy interaction is at least qualitatively in accordance with simple electrostatics, the vacancy-dopant interaction is in qualitative contradiction with electrostatics and indirectly affects the vacancy-vacancy interaction in a profound way. It is thus clear that the complexity of defect ordering in YSZ stretches beyond mere electrostatic effects.

Several semiempirical studies have recently pointed out that the defect ordering is affected by long-range relaxations in the ionic crystal.[44,45] Within these studies, it was found that the anion relaxation into the vacancy depended strongly on the size of the dopant ion, presenting a size-dependent argument for why anion vacancies would prefer to bind to one or the other of two different-sized cations. Recent first-principles calculations show that anion-cation ordering in cubic-stabilized zirconia is dictated by elastic interactions, which are strong enough to overcome electrostatic forces.[57]

TABLE II. Energetic and structural information for the six cation configurations within the $Zr_2Y_2O_7$ stoichiometry. Given are the formation enthalpies $\Delta H$ (eV/cation) for the lowest-energy vacancy placement in each cation configuration, as computed within DFT-GGA. The nearest-neighbor cation pair correlation $\alpha$ (analogous to the Warren-Cowley short-range order parameter) indicates the number of unlike nearest-neighbor cation-cation pairs, with negative (positive) values indicating the propensity for Zr-Y (Zr-Zr and Y-Y) bonds. $n_{Zr}$ and $n_Y$ are the local coordination numbers (i.e., the number of oxygen neighbors) for each of the four cations in the cell. The notation in the leftmost column is for these purposes just meant to identify the different cation structures, and the superlattice stackings and orientations are given.

| Structure | Cation superlattice | $n_{Zr}$ | $n_Y$ | $\Delta H$ (eV) | $\alpha$ |
|---|---|---|---|---|---|
| W2 | $Zr_2Y_2$ ⟨311⟩ | 7,6 | 8,7 | −0.018 | −1/6 |
| Y2 | $Zr_2Y_2$ ⟨110⟩ | 7,6 | 8,7 | +0.080 | 0 |
| CH | $Zr_2Y_2$ ⟨210⟩ | 7,7 | 7,7 | +0.088 | −1/3 |
| V2 | $Zr_2Y_2$ ⟨111⟩ | 8,8 | 7,5 | +0.207 | +1/2 |
| Z2 | $Zr_2Y_2$ ⟨100⟩ | 8,8 | 6,6 | +0.331 | +1/3 |
| CA | $Zr_1Y_1$ ⟨100⟩ | 8,6 | 8,6 | +0.371 | −1/3 |

#### *3. Dopant-dopant interactions*

The interactions between dopants on the cation sublattice is a virtually unknown subject. Scattering experiments have difficulty in distinguishing between Zr and Y ions, and almost no theoretical work has been devoted to this issue. X-ray scattering data for zirconia stabilized with other trivalent metal ions with a higher contrast difference to Zr ions have suggested that there are indeed ordering tendencies also on this sublattice.[53]

Since there are only two distinctly different cation ordering possibilities for the rhombohedral $Zr_3Y_4O_{12}$ compound, this is not a very instructive case to assess dopant-dopant interactions (despite the large number of anion ordering possibilities). The composition that best serves our purposes here is that of the pyrochlore ($Zr_2Y_2O_7$) structure, where we have considered six different cation ordering possibilities. For each cation configuration, a symmetry analysis was undertaken to isolate all possible inequivalent vacancy sites, and first-principles calculations were then performed for all of these configurations. The formation enthalpies corresponding to the lowest-energy vacancy placement within each cation arrangement and nearest-neighbor pair correlation are given in Table II. From this limited amount of data, the following conclusions can be drawn: (i) The energetic consequences of cation ordering are substantial, as noted from the large spread in energies, and (ii) the ordering effect is not ''simple,'' since it does not follow the nearest-neighbor correlation. (iii) There is a clear energetic preference for lower coordination of $Zr^{4+}$ and higher coordination

of $Y^{3+}$ by oxygen ions. This fact is again a manifestation of the energetic tendency for $Zr^{4+}$-□ association. (iv) The lowest-energy structure, ''W2,'' has a ⟨311⟩ cation superlattice stacking, consistent with the ⟨311⟩ low-energy W1 superlattice found for the $Zr_6Y_2O_{15}$ composition. This preference for ⟨311⟩ structures in the fluorite based lattice should be contrasted against the preference for other cation orientations (⟨100⟩, ⟨111⟩, and ⟨210⟩) found in fcc, rocksalt, and zinc-blende based systems (see Ref. 58). Beyond these four statements, it is not possible with the present body of data to establish any quantitative statements about dopant-dopant interactions. The complication is that the vacancy-vacancy, vacancy-dopant, and dopant-dopant interactions are all coupled, and in principle often inseparable. For instance, one might argue that since vacancies repel one another, and are attracted to Zr more than to Y, the □-□ and □-dopant interactions indirectly cause the Zr ions to separate from one another as much as possible (i.e., the Y ions also separate from one another as much as possible). Thus, it is difficult to establish with certainty whether the cations order due to electrostatic repulsion between like cations or if the like cations simply are ''dragged apart'' by the ordering on the anion and anion-cation lattice.

Since there is no easy diffusion channel for the cations, their mobility is orders of magnitude lower than the anion mobility, which is facilitated by the charge compensating vacancies. Thus, the cation ordering is much more sluggish than the anion ordering, and therefore more prone to be sensitive to the processing of the electrolyte. Depending on the specific preparation and thermal history of the electrolyte material, it is therefore likely that one will obtain a system in partial equilibrium, in which the cation (Zr-dopant) distribution is kinetically frozen into nonequilibrium configurations. Meanwhile, the anions are typically sufficiently mobile during this process to adapt to whatever (short-range and/or long-range ordered) cation configuration is reached in the process of minimizing the free energy of the system. These considerations add to the lack of experimental consensus on the dopant-dopant ordering in stabilized zirconia.

We conclude this section by noting that the above results bear significant implications for the deterioration of ionic conduction upon thermal aging. It is clear at this point that part of the aging process can be reversed by high-temperature exposure, as noted in recent YSZ experiments.[21] On the other hand, it is also quite clear that part of the aging process is irreversible since the system always strives to lower its free energy, also noted repeatedly in conduction experiments.[3,21] In the absence of a detailed thermal analysis of the YSZ system, it is premature to draw specific conclusions about the connections between defect ordering and thermal aging in YSZ electrolytes. It does seem likely, however, that both reversible and irreversible aging are intimately connected with (short-range and long-range) anion and cation ordering in the solid solution of stabilized cubic zirconia. We are currently developing a coupled-cluster-expansion scheme[47] to investigate finite-temperature ordering phenomena using Monte Carlo techniques.

## V. OTHER ALIOVALENT DOPANTS

The rationale behind choosing yttria-stabilized zirconia as the electrolyte material in many electrochemical devices is its combination of high ionic conductivity and chemical stability under a wide range of partial oxygen pressures. Although there are a number of electrolytes with a higher ionic conductivity, none of them has yet been shown to be as stable as zirconia-based electrolytes with respect to thermal aging and oxidizing or reducing environments. There is thus great incentive to learn whether other dopants or dopant combinations can increase the ionic conductivity, while maintaining the chemical integrity and other appealing properties of YSZ.

Experimental studies of aliovalent dopants other than yttria in the cubic phase of zirconia have been plentiful. Although there are often quantitative discrepancies between reported conductivity data, mainly due to differences in sample preparation and thermal history of the electrolyte (see Refs. 3 and 21 for a comprehensive review), the qualitative features seem firmly established: The dopant ions besides $Y^{3+}$ that yield the highest conductivity in cubic zirconia, especially in fresh (unaged) samples, are the late lanthanides and $Sc^{3+}$, which has been reported to surpass even $Y^{3+}$ in terms of ionic conductivity.[3] However, there is no one dopant candidate that clearly stands out as being superior overall to the performance of YSZ. Given the number of possible additive alternatives, the often poorly known phase diagrams of these oxide systems, and the wide range of concentrations to be sampled, it is clear that a purely Edisonian approach is likely to be inefficient. If zirconia systems with more than one added oxide component are considered, an unguided approach becomes quite intractable. By extracting trends from experimental results, one can try to gain some insight into what properties of a dopant make for a highly conducting electrolyte. Several systematic studies have found a strong correlation between electrolyte conductivity and the ionic radius of the dopant ion. Experimental studies have measured a monotonically increasing conductivity with decreasing ion size,[3,59] while semiempirical calculations seem to suggest that the ionic conductivity peaks out for dopants with intermediate radii (namely, near that of the zirconia ion).[44,45] Here we employ highly accurate and predictive first-principles calculations to gain some insight into these matters and assess the validity of less accurate empirical models. To keep the problem tractable, we capitalize on our newly gained insight into the mixed defect ordering of YSZ (Sec. IV) to carefully choose an ensemble of calculations for a selected set of trivalent and divalent dopant oxides.

### A. Prototype structure

As a representative structure, we choose the W1 superlattice as described in Sec. IV A 2: This structure consists of a $Zr_3/X_1$ cation stacking along ⟨311⟩ (where $X$ represents the dopant ion), and corresponds to the low-energy $Zr_6Y_2O_{15}$ structure found in Fig. 2. The oxygen ions (and vacancies) are placed in the fluorite positions. By altering the placement of the vacant anion sites, this structure affords the possibility of examining several distinct vacancy-dopant geometries.

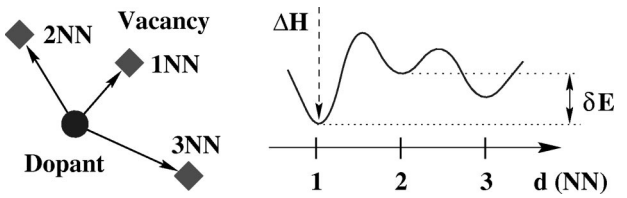


FIG. 4. Schematic illustration of the variations in vacancy-dopant binding $\delta E$ as an anion vacancy traverses the oxide.

In the case of the trivalent dopants, we replace two Zr ions with two dopant ions and remove one oxygen ion from the oxygen sublattice. Thus the W1 structure with trivalent dopants $T^{3+}$ corresponds to a stoichiometry of $Zr_6T_2O_{15}$. Within this trivalent W1 structure, there are three substructures with varying vacancy-dopant distance, from first to third neighboring coordination shells. In the case of the divalent dopant ion, $D^{2+}$, we begin with the same W1 cell shape, but now substitute only one Zr ion for one dopant ion and simultaneously create one anion vacancy for charge compensation. This subsitution gives a stoichiometry of $Zr_7D_1O_{15}$ for the divalent dopants. Within this modification of the W1 structure, we now find four different ways to arrange the dopant ion with respect to the anion vacancy. For each of the trivalent and divalent dopants, we compute the enthalpy of formation for all vacancy-dopant arrangements. We then focus on three quantities for each dopant as the vacancy-dopant distance is changed (as illustrated schematically in Fig. 4): (1) the overall lowest value for the formation enthalpy $\Delta H_{W1}$ (Fig. 5), (2) the preferred vacancy-dopant separation $\delta E^*_{W1}$ (Fig. 6), as defined below, and (3) the overall maximum change in binding $\delta E_{W1}$ (Fig. 7). Although the choice of W1 cation superlattice may seem a bit arbitrary, we have found this structure to be energetically favorable in the YSZ system, and as we show below, it serves to demonstrate the generic ordering tendencies for a wide variety of dopant systems.

### B. Formation enthalpies

The formation enthalpies for an ensemble of trivalent and divalent dopants corresponding to the lowest-energy vacancy

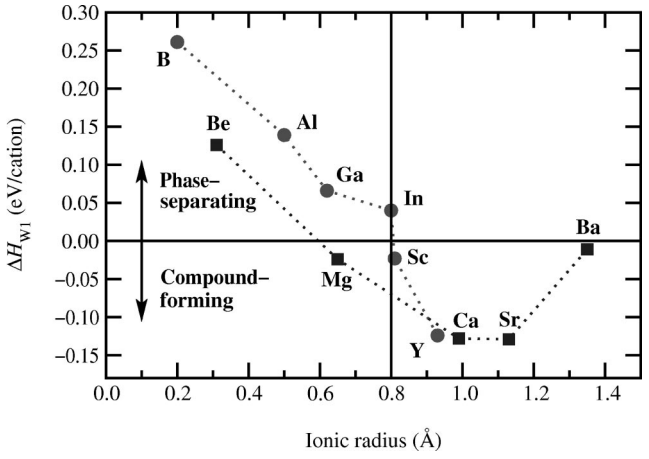


FIG. 5. Formation enthalpies (eV/cation) for trivalent and divalent dopants in the $Zr_6Y_2O_{15}$ W1 structure, as computed within DFT-GGA.

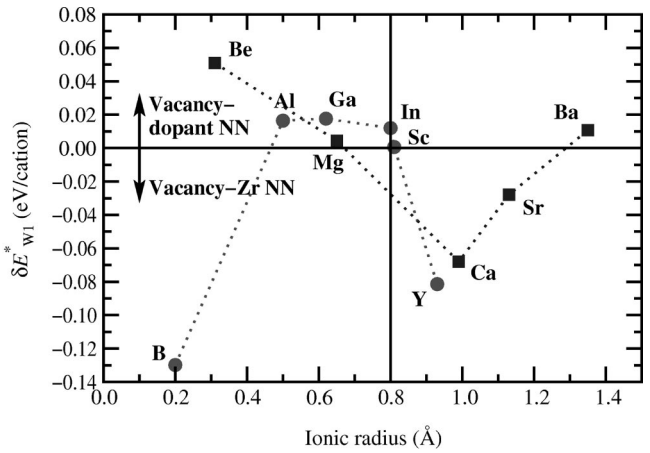


FIG. 6. Difference in formation enthalpy (eV/cation) between 1NN and 3NN vacancy-dopant arrangements for trivalent and divalent dopants in the $Zr_6Y_2O_{15}$ W1 structure as computed within DFT-GGA.

positions in the W1 structure are shown in Fig. 5 as a function of ionic dopant radius. Note that these energies are all computed with respect to cubic zirconia and the respective constituent dopant oxide, and that the ionic radii, which are not exactly well defined, are all taken from a single source (Ref. 60) for consistency. A clear trend emerges from this figure: The formation enthalpy is always positive (indicative of a phase-separating tendency) for dopants with radii distinctly different from that of $Zr^{4+}$, with the most positive values for small dopant ions. For dopants with an ionic radius near that of $Zr^{4+}$ or slightly larger, however, the formation enthalpy is always negative, indicating the stability of compound formation with respect to phase separation. Thus, only for ''size-matched'' (or slightly larger) dopant ions does one obtain long-range ordering in zirconia-based systems.

This calculated trend is entirely consistent with the experimentally determined phase diagrams:[61] $ZrO_2$ stabilized

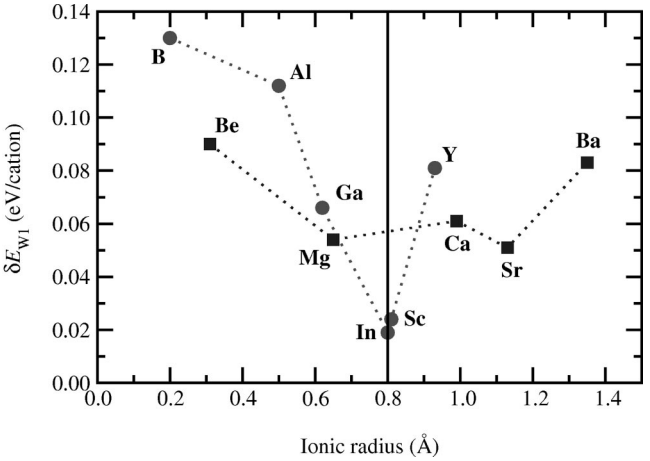


FIG. 7. Maximal variations in the dopant-vacancy binding energy (eV/cation) as the vacancy-dopant separation is increased from 1NN to 3NN for a number of divalent and trivalent dopants in the $Zr_6Y_2O_{15}$ W1 structure of zirconia.

with $Y_2O_3$, $Sc_2O_3$, CaO, SrO, and BaO all show observed ordered compounds where our calculations yield $\Delta H_{W1}<0$. On the other hand, $ZrO_2$ doped with BeO and $Al_2O_3$ shows phase separation in the measured phase diagrams, consistent with our calculations of $\Delta H_{W1}>0$. We are not aware of experimental information concerning the compound-forming versus phase-separating tendencies of the $ZrO_2$-$B_2O_3$, $ZrO_2$-$Ga_2O_3$, or $ZrO_2$-$In_2O_3$ systems, although our calculations yield $\Delta H_{W1}>0$ for each of these systems in the W1 structure. In the $ZrO_2$-MgO system, although the measured phase diagram[61] shows no ordered compounds, our calculations for the W1 $Zr_7MgO_{15}$ structure produce a slightly negative formation enthalpy. Thus, our calculations demonstrate that as-yet-unobserved ordered compounds likely exist in the $ZrO_2$-MgO system at low temperatures, but from our present calculations, we cannot predict the finite-temperature stability of these phases.

The formation enthalpy tendencies of Fig. 5 give a global indication of compound-forming versus phase-separating *long-range ordering* tendencies in an alloy system. The stable long-range order involves energy differences between compounds with different compositions, such as the formation enthalpy of Eq. (1). However, to understand the local effects of *short-range defect ordering* in these systems, we must examine the energetics of various configurations of defects, all at the same composition. This distinction between long- and short-range ordering and the contributing energy differences involved has been discussed in detail for metallic and semiconducting systems.[55]

### C. Defect ordering

In Sec. IV, we establish that first-principles calculations and the majority of recent experimental studies show that anion vacancies in YSZ prefer to associate with host ions rather than the dopant ions, despite earlier reports of the opposite ordering. The natural question then is to ask whether this is a general behavior, or particular to the case of YSZ. EXAFS studies have demonstrated that vacancies prefer Zr coordination when the zirconia is doped with the small-radius cation erbium and dopant coordination in the case of the large-radius cation lanthanum.[17] Given the vast disagreements in the literature of the much more well-studied YSZ, one might be tempted to question the conclusiveness of this observation. However, recent semiempirical calculations[44,45] corroborate these ideas, showing that vacancies actually prefer to associate with the dopant ions rather than Zr host ions, if the dopants are small enough (smaller than the Zr ion). Our calculations for the W1 structure let us independently assess this issue from first principles for a number of divalent and trivalent dopants. In both sets of calculations, the individual and average (there are two dopant cations and one vacancy per W1 cell) vacancy-dopant separations vary from 1NN to 3NN, depending on the placement of the vacancy in the cell. Although the number of studied configurations for each individual dopant is significantly smaller than in our extensive YSZ study, we still expect to discern changes in the energetically preferred vacancy-dopant separation preference as the ionic radii varies with dopant.

For these purposes, we compute the difference in the formation enthalpy between the W1 1NN and 3NN vacancy-dopant configuration for each dopant, and plot these results in Fig. 6. This analysis shows a clear preference for vacancy-dopant association for dopants with small radii and vacancy-Zr association for large dopants, with the crossover point right at the radius of Zr—all in excellent agreement with semiempirical studies.[44,45] The one significant exception to this clear trend comes from the smallest of the considered dopants, B, which is also the dopant with the highest formation enthalpy (i.e., most unfavorable) in the W1 structure. In addition, the largest of the considered dopants, Ba, shows a slight energetic preference to go against this trend as well. It is unclear at this point whether this is just an artifact of our limited sampling and large span of considered ionic radii or if possibly the vacancy-dopant association tendencies are even more complicated than first anticipated.

### D. Vacancy-dopant binding vs ionic conductivity

To determine the variations in the binding strength of the vacancy-dopant complexes in each of the aliovalently doped systems, we next compute the maximum change in binding energy $\delta E_{W1}$ as the vacancy position and the concomitant vacancy-dopant separation is changed (from 1NN to 2NN to 3NN) as illustrated in Fig. 4. These variations in the vacancy-dopant binding energies are shown in Fig. 7 as a function of the ionic radius of the dopants. Again, a clear trend emerges from these results: the smallest variation in the binding energy between dopant ions and vacancies occurs for dopants which are nearly ''size matched'' with $Zr^{4+}$. This trend in the binding energy has important implications towards understanding the ionic conductivity in these systems. For systems with a very small binding energy variation (e.g., $Sc_2O_3$-doped $ZrO_2$), the vacancies are unlikely to become bound at any particular coordination shell to a cation site because there is no particular vacancy-dopant arrangement that is preferred over another. Interestingly, the same trend was reported in a recent semiempirical study,[45] demonstrating the utility of such considerably simpler theoretical descriptions. The good agreement between semiempirical and first-principles studies might be unexpected for such a highly complex mixed ionic-covalent system, particularly given that previous attempts at describing conceptually simpler aluminum oxides using similar interatomic potentials have been considerably less successful. As discussed in Ref. 57, the likely explanation comes from the fact that the *relative* ordering tendencies between different isovalent dopants in zirconia are largely governed by elastic interactions, which are easier to capture in model descriptions than complex electronic interactions.

At low electrolyte temperatures, bulk anion mobility is dictated primarily by kinetic barriers to vacancy diffusion. As the electrolyte temperature is increased, however, vacancy hopping becomes sufficiently fast so that the relative binding of the vacancy with regard to the dopant environ-

ment starts to play an increasingly more important role. Thus, especially at high temperatures, a small binding bias should be indicative of a high ionic conductivity, as first pointed out in semi-empirical studies.[44,45] Indeed, the $Sc_2O_3$-stabilized zirconia system, which has one of the smallest binding biases in our study, has the highest conductivity of any known binary doped zirconia. Other systems also observed to possess relatively high conductivities ($Y_2O_3$- and CaO-doped) also are calculated to have a relatively small vacancy-dopant binding variation. Furthermore, all of the late lanthanide stabilizers experimentally noted to yield good ionic conductivity in cubic zirconia[3] fit perfectly into this simple model in terms of valency characteristics and ionic size. These considerations also suggest that $Al_2O_3$ and $B_2O_3$ doping of $ZrO_2$ are likely to produce vacancies which are strongly bound to certain cation sites, and therefore, likely poor conductors.

In addition to explaining well-established experimental trends, our calculations also point to another particularly promising dopant material: from Fig. 7 we note that $In_2O_3$-doped $ZrO_2$ parallels the $Sc_2O_3$ system in terms of having a small binding energy variation with respect to different vacancy-dopant separations. Thus, within the assumptions outlined above, we highlight $In_2O_3$ as a dopant likely to produce high ionic conductivity in cubic zirconia. Another interesting point in favor of $In_2O_3$-doped $ZrO_2$ is that the $\Delta H$ of the ordered $Zr_6In_2O_15$ compound in Fig. 5 is *positive*, whereas it is negative in both the $Sc_2O_3$ and $Y_2O_3$ doped systems. This could indicated that $In_2O_3$-doped $ZrO_2$ is less susceptible to ordering tendencies, which can degrade conductivity and lead to deleterious aging effects. While a more extensive investigation of $In_2O_3$-doped $ZrO_2$ (ISZ) would have to be performed to more firmly establish these conclusions, our preliminary results point to a less ordered solid solution phase in ISZ than in YSZ or ScSZ. The few existing (experimental) reports on the conductivity of $In_2O_3$-doped $ZrO_2$,[62–64] all report a high conductivity in this system, comparable or even better than that of YSZ. Further investigation of this dopant system is thus justified, especially since ionic conduction in ISZ has not been nearly as well studied (or optimized) as in YSZ. Finally, we note that while we do not find any defect states in the band gap of the few representative structures of $In_2O_3$-stabilized zirconia (or any other of the dopant systems considered here for that matter), this particular system has been noted to exhibit a small degree of electronic conduction (ionic transference number $>0.9$) at higher dopant concentrations.

At this point, one might wonder how a few select thermodynamic calculations can possibly capture the complex kinetic phenomenon of ionic conduction in defect-stabilized oxides. Clearly, these first-principles (parameter-free) calculations present some persuasive arguments that this is indeed possible by correctly identifying the experimentally established best ionic conductors. To complement our thermodynamic considerations, we have embarked on a kinetic study of ionic conduction in YSZ. Specifically, we have used a sophisticated transition-state search technique (the nudged elastic band method[65]) to compute the activation energies for vacancy-mediated oxygen diffusion in YSZ electrolytes.

TABLE III. Compilation of theoretical and experimental results for the relative energetic ordering of the three zero-pressure zirconia phases. Energy differences are given with respect to the cubic phase in units of meV/cation. A negative value of $\delta E_{t-c}$ ($\delta E_{m-c}$) indicates a higher formation enthalpy for the tetragonal (monoclinic) over the cubic phase. The leftmost column indicates the exchange-correlation functional, the next one the choice of basis sets for expanding the wavefunction (PW-PP=plane-wave pseudopotential, FLMTO=full potential linear muffin-tin orbital).

| XCF | Method | Reference | $\delta E_{t-c}$ | $\delta E_{m-c}$ |
|---|---|---|---|---|
| Expt. | | 69 | −57 | −120 |
| LDA | PW-PP | Present work | −35 | −82 |
| | PW-PP | 32 | −20 | −60 |
| | PW-PP | 36 | −45 | −102 |
| | PW-PP | 34 | −48 | −112 |
| | FLMTO | 29 | −49 | −105 |
| | PW-PP | 30 | +99 | −46 |
| GGA-PW91 | PW-PP | Present work | −82 | −188 |
| | PW-PP | 32 | −80 | −170 |
| GGA-PBE | PW-PP | 32 | −80 | −190 |
| HF | | 41 | −8 | +5 |

Since the number of possible defect arrangements even at a single composition is very large and first-principles diffusion barriers are prohibitively computer intensive, we have only started to unravel the mechanisms, anisotropies, and activation energies, for vacancy diffusion in stabilized zirconia. From several such calculations for the $Zr_3Y_4O_{12}$ composition we can so far formulate the following conclusions: (i) the vacancy diffusion is highly anisotropic, (ii) it often involves a considerable distortion of the ionic lattice, and (iii) the range of computed activation energies is quite wide, yet so far limited to about 1.4 eV. These barriers are of the same order as the effective activation energies measured in standard 8–10 mol % YSZ electrolytes, about 0.7–1.2 eV, depending on the thermal history of the oxide.[3,5] To put these numbers in perspective, a diffusion process with an activation energy of 0.7 (1.2) eV occurs on the order of once every picosecond (nanosecond) at an electrolyte temperature of 1000 °C (assuming a normal prefactor of about $10^{13}$ $s^{-1}$ and ignoring geometrical influences).[66] Thus, even processes with a ''large'' barrier happen quite readily at such elevated temperatures, typical in electrolyte applications. Consequently, it is not so surprising that experimental (impedance spectroscopy) studies often find that the rate-limiting process in state-of-the-art (anode supported thin-film electrolyte) solid-oxide fuel cells often is contained in electrolyte/cathode or electrolyte/anode interface processes rather than solely in bulk electrolyte vacancy diffusion.[67,68]

## VI. CONCLUSIONS

In summary, we have combined powerful lattice algebra techniques with modern state-of-the-art first-principles density functional calculations to clarify the ordering and clustering tendencies in yttria-stabilized zirconia. We have then used these findings to assess the vacancy binding preferences

TABLE IV. Comparison between LDA and GGA formation enthalpies for the YSZ pyrochlores with and without including *p* electrons in the valence. Note that the formation enthalpies are quite generally shifted down in the GGA.

| | LDA | | GGA | |
|---|---|---|---|---|
| Structure | $\Delta H_c$ | $\Delta H_v$ | $\Delta H_c$ | $\Delta H_v$ |
| CH | 0.177 | 0.127 | 0.130 | 0.088 |
| Y2.a | 0.155 | 0.121 | 0.117 | 0.080 |
| Y2.b | 0.167 | 0.144 | 0.147 | 0.123 |
| V2.a | 0.536 | 0.471 | 0.450 | 0.383 |
| V2.b | 0.309 | 0.278 | 0.275 | 0.240 |
| V2.c | 0.254 | 0.226 | 0.239 | 0.207 |
| V2.d | 0.529 | 0.465 | 0.444 | 0.376 |
| Z2.a | 0.710 | 0.600 | 0.633 | 0.525 |
| Z2.b | 0.615 | 0.507 | 0.565 | 0.457 |
| Z2.c | 0.395 | 0.331 | 0.397 | 0.331 |
| W2.a | 0.062 | 0.051 | 0.042 | 0.029 |
| W2.b | 0.160 | 0.141 | 0.136 | 0.112 |
| W2.c | 0.062 | 0.045 | 0.015 | −0.006 |
| W2.d | 0.039 | 0.027 | −0.003 | −0.018 |

for a suite of other trivalent and divalent dopants in addition to $Y^{3+}$. We find that anion vacancies in YSZ repel each other at short separations, but show an energetic preference to align as third nearest neighbors along ⟨111⟩ directions, in excellent agreement with neutron scattering measurements. We also find a strong energetic dependence on cation configuration. Regarding vacancy-dopant interactions, the anion vacancies prefer to be close to the smaller of the two cations, i.e., close to Zr ions in the case of over-sized dopants and close to the dopants otherwise. With dopant cations similar in size to $Zr^{4+}$, the vacancies show no particular preference, and are thus less prone to be tied up by the cations when traversing such oxides. This lack of a strong preference for the vacancy-dopant separation offers some simple insight into the high conductivity of, e.g., $Sc_2O_3$- and $Y_2O_3$-doped zirconia, and points out $In_2O_3$ as a particularly promising zirconia dopant for high ionic conductivity.

Of particular interest here is that we in this systematic study are able to establish the complete crystal structure (including all atomic positions) of the only ordered structure observed experimentally, $\delta$-$Zr_3Y_4O_{12}$. By applying lattice algebra techniques, we reduce the vast number of possible structures to only 45 candidates, and then isolate the ground-state structure using first-principles calculations. The structure we identify as the $\delta$-$Zr_3Y_4O_{12}$ phase (given in the Appendix) has its vacancies as third nearest neighbors along ⟨111⟩. Thus, the lowest-energy structure of this ordered compound follows the same rules we find for the solid solution range. In this study, we also discover new metastable Zr-rich phases which have yet to be experimentally confirmed. Such confirmation very much depends on how high in temperature these structures are stable.

## ACKNOWLEDGMENTS

We gratefully acknowledge stimulating discussions with D. Raczkowski.

TABLE V. Ionic coordinates for the $\delta$-$Zr_3Y_4O_{12}$ structure, as computed within DFT-GGA. The fully relaxed cation and anion coordinates, as well as the ideal anion vacancy positions $s_1$-$s_3$, are given in scaled (direct) space, with the matrix multiplier (unit cell vectors) for conversion to Cartesian coordinates provided in the first three lines ($\mathbf{a}_1$–$\mathbf{a}_3$), in units of Å. The last column shows the coordination number *n* for cations, anions, and anion vacancies.

| Unit cell vectors | | | | |
|---|---|---|---|---|
| $\mathbf{a}_1$ | 5.2832 | 2.6498 | 2.6099 | |
| $\mathbf{a}_2$ | −2.6055 | 5.2569 | 2.5793 | |
| $\mathbf{a}_3$ | −2.6754 | −2.7939 | 5.4271 | |
| Ion | $s_1$ | $s_2$ | $s_3$ | *n* |
| $Zr_1$ | 0.4600 | 0.1331 | 0.7602 | $O_7$ |
| | 0.2543 | 0.4384 | 0.0969 | $O_7$ |
| $Zr_2$ | 0.8571 | 0.2857 | 0.4286 | $O_6$ |
| $Y_1$ | 0.9913 | 0.9829 | 0.0391 | $O_7$ |
| | 0.7230 | 0.5885 | 0.8180 | $O_7$ |
| $Y_2$ | 0.1580 | 0.6715 | 0.5623 | $O_7$ |
| | 0.5563 | 0.8999 | 0.2948 | $O_7$ |
| $O_1$ | 0.2874 | 0.1144 | 0.0036 | $Zr_2Y_2$ |
| | 0.4269 | 0.4571 | 0.8536 | |
| $O_2$ | 0.6678 | 0.8736 | 0.9941 | $Zr_1Y_3$ |
| | 0.0465 | 0.6978 | 0.8630 | |
| $O_3$ | 0.7690 | 0.2072 | 0.7326 | $Zr_2Y_2$ |
| | 0.9453 | 0.3642 | 0.1246 | |
| $O_4$ | 0.1781 | 0.3066 | 0.5482 | $Zr_3Y_1$ |
| | 0.5362 | 0.2648 | 0.3089 | |
| $O_5$ | 0.4408 | 0.8713 | 0.6083 | $Zr_1Y_3$ |
| | 0.2735 | 0.7002 | 0.2488 | |
| $O_6$ | 0.7922 | 0.6004 | 0.4879 | $Zr_1Y_3$ |
| | 0.9221 | 0.9711 | 0.3692 | |
| $\square_1$ | 0.1071 | 0.0357 | 0.6786 | $Zr_2Y_2$ |
| $\square_2$ | 0.6071 | 0.5357 | 0.1786 | $Zr_2Y_2$ |

## APPENDIX

In this appendix, we summarize some technical results for the interested reader. Table III contains a comparison between different theoretical studies (and methods) regarding the formation enthalpies of the three pure zirconia polymorphs (monoclinic, tetragonal, and cubic). Our own results are in excellent agreement with the most recent of these studies.

Table IV contains the formation enthalpies for all of the YSZ pyrochlore structures considered in this study. Four sets of computations were made:

LDA-CA, *p* electrons pseudized in the core,

LDA-CA, *p* electrons in the valence,

GGA-PW91, *p* electrons pseudized in the core,

GGA-PW91, *p* electrons in the valence.

The general trend of explicitly including semicore states in the valence is a systematic downshift of formation enthalpies (towards more favorable enthalpies). The same trend is noted

when gradient corrections are included. However, in all four sets of calculations, the relative energies are quite similar, indicating that the qualitative trends are unlikely to be affected by XC or treatment of semicore states.

Table V gives the cell vectors and complete ionic positions (both cations and anions) for the first-principles predicted lowest-energy $\delta$-$Zr_3Y_4O_{12}$ structure. Experimental investigations of the $\delta$ phase have not yielded complete, fully occupied cation positions, but rather some partial (Zr,Y) occupations resulting in a relatively high-symmetry rhombohedral space group. Our first-principles calculations give the complete cation ordering and therefore necessarily yield a low symmetry cell, which we find to be triclinic. We have not attempted to find the space group of this structure, but simply give the cell vectors in Cartesian coordinates (in Å) and all the ionic positions in fractional (i.e., direct, not Cartesian) coordinates in terms of the three cell vectors. We also indicate the ions which we find to be symmetry equivalent (i.e., those with the same Wyckoff position).


[1] W. Nernst, U.S. Patent 685730 (1902) (filed 8/24/1899); Z. Elektrochem. **6**, 41 (1900).

[2] C. Wagner, Naturwissenschaften **31**, 265 (1943).

[3] V. V. Kharton, E. N. Naumovich, and A. A. Vecher, J. Solid Electrochem. **3**, 61 (1999); V. V. Kharton, A. A. Yaremchenko, and E. N. Naumovich, *ibid.* **3**, 303 (1999).

[4] A. J. McEvoy, Solid State Ionics **132**, 159 (2000).

[5] T. H. Etsell and S. N. Flengas, Chem. Rev. **70**, 339 (1970).

[6] Note that the use of the word ''dopant'' here refers to the non-Zr cation in these materials (e.g., Y in the case of YSZ). It is not meant to imply any restriction on the composition of the material or that the dopant level must necessarily be dilute. ''Additive'' or ''stabilizer'' are synonymous for the purposes of this paper.

[7] T. Y. Tien and E. C. Subbarao, J. Chem. Phys. **39**, 1041 (1963).

[8] A. Nakamura and J. B. Wagner, Jr., J. Electrochem. Soc. **127**, 2325 (1980); **133**, 1542 (1986).

[9] H. Schmalzried, Z. Phys. Chem., Neue Folge **105**, 47 (1977).

[10] D. Steele and B. E. F. Fender, J. Phys. C **7**, 1 (1974).

[11] W. L. Roth, R. Wong, A. I. Goldman, E. Canova, Y. H. Kao, and B. Dunn, Solid State Ionics **18-19**, 1115 (1986).

[12] M. H. Tuilier, J. Dexpert-Ghys, H. Dexpert, and P. Lagarde, J. Solid State Chem. **69**, 153 (1987).

[13] H. Morikawa, Y. Shimizugawa, F. Marumo, T. Harasawa, H. Ikawa, K. Tohji, and Y. Udagawa, J. Jpn. Ceram. Soc. **96**, 253 (1988).

[14] Z. J. Shen, T. K. Li, K. Q. Lu, and Y. Q. Zhao, Guisuanyan Xuebao **16**, 270 (1988).

[15] X. Li and B. Hafskjold, J. Phys.: Condens. Matter **7**, 1255 (1995).

[16] C. R. A. Catlow, A. V. Chadwick, G. N. Greaves, and L. M. Moroney, J. Am. Ceram. Soc. **69**, 272 (1986).

[17] M. Cole, C. R. A. Catlow, and J. P. Dragun, J. Phys. Chem. Solids **51**, 507 (1990).

[18] F. Shimojo, T. Okabe, F. Tachibana, M. Kobayashi, and H. Okazaki, J. Phys. Soc. Jpn. **61**, 2848 (1992).

[19] P. Li, I-W. Chen, and J. E. Penner-Hahn, Phys. Rev. B **48**, 10 074 (1993); J. Am. Ceram. Soc. **77**, 118 (1994).

[20] J. P. Goff, W. Hayes, S. Hull, M. T. Hutchings, and K. N. Clausen, Phys. Rev. B **59**, 14 202 (1999).

[21] J. Kondoh, T. Kawashima, S. Kikuchi, Y. Tomii, and Y. Ito, J. Electrochem. Soc. **145**, 1527 (1998); J. Kondoh, S. Kikuchi, Y. Tomii, and Y. Ito, Physica B **262**, 177 (1999).

[22] P. Hohenberg and W. Kohn, Phys. Rev. **136**, B864 (1964).

[23] W. Kohn and L. J. Sham, Phys. Rev. **140**, A1133 (1965).

[24] D. Vanderbilt, Phys. Rev. B **32**, 8412 (1985).

[25] G. Kresse and J. Hafner, Phys. Rev. B **47**, 558 (1993); **49**, 14 251 (1994); **54**, 11 169 (1996).

[26] J. P. Perdew, in *Electronic Structure of Solids 1991*, edited by P. Ziesche and H. Eschrig (Akademie-Verlag, Berlin, 1991), Vol. 11.

[27] D. M. Ceperley and B. J. Alder, Phys. Rev. Lett. **45**, 566 (1980); J. P. Perdew and A. Zunger, Phys. Rev. B **23**, 5048 (1981).

[28] H. F. Jansen, Phys. Rev. B **43**, 7267 (1991).

[29] M. W. Finnis, A. T. Paxton, M. Methfessel, and M. van Schilfgaarde, Phys. Rev. Lett. **81**, 5149 (1998).

[30] J. K. Dewhurst and J. E. Lowther, Phys. Rev. B **57**, 741 (1998).

[31] A. Christensen and E. A. Carter, Phys. Rev. B **58**, 8050 (1998).

[32] G. Jomard, T. Petit, A. Pasturel, L. Magaud, G. Kresse, and J. Hafner, Phys. Rev. B **59**, 4044 (1999).

[33] S. Gennard, F. Corá, and C. R. A. Catlow, J. Phys. Chem. B **103**, 10 158 (1999).

[34] G. Stapper, M. Bernasconi, N. Nicoloso, and M. Parrinello, Phys. Rev. B **59**, 797 (2000).

[35] K. Parlinski, Z. Q. Li, and Y. Kawazoe, Phys. Rev. Lett. **78**, 4063 (1997).

[36] B. Kralik, E. K. Chang, and S. G. Louie, Phys. Rev. B **57**, 7027 (1998).

[37] R. W. G. Wyckoff, *Crystal Structures*, 2nd ed. (Wiley, New York, 1963 and 1964), Vols. 1 and 2.

[38] We also considered the divalent dopant PtO. In computing the transition-metal oxide PtO in the cooperite structure, we found that the material is predicted to be a metal in the DFT calculations rather than an insulator. Therefore, we chose not to perform calculations of $ZrO_2$-PtO analogous to the other divalent systems.

[39] C. J. Howard, R. J. Hill, and B. E. Reichert, Acta Crystallogr., Sect. B: Struct. Sci. **44**, 116 (1988). These neutron diffraction observations are not for the pure oxide, but for samples of monoclinic $ZrO_2$, tetragonal $Zr_{0.935}Y_{0.065}O_{1.968}$, and cubic $Zr_{0.875}Mg_{0.125}O_{1.875}$.

[40] V. S. Stubican, J. R. Hellmann, and S. P. Ray, Mater. Sci. Monogr. **10**, 257 (1982).

[41] E. V. Stefanovich, A. L. Shluger, and C. R. A. Catlow, Phys. Rev. B **49**, 11 560 (1994).

[42] S. Chandra, *Superionic Solids: Principles and Applications* (North-Holland, Amsterdam, 1981).

[43] E. C. Subbarao, in *Science and Technology of Zirconia*, edited by A. H. Heuer (American Ceramic Society, Columbus, OH, 1981).

[44] M. Sakib Khan, M. Saiful Islam, and D. R. Bates, J. Mater. Chem. **8**, 2299 (1998).

[45] M. O. Zacater, L. Minervini, D. J. Bradfield, R. W. Grimes, K. E. Sickafus, Solid State Ionics **128**, 243 (2000).
[46] G. Ceder, A. F. Kohan, M. K. Aydinol, P. D. Tepesch, and A. Van der Ven, J. Am. Ceram. Soc. **81**, 517 (1998).
[47] P. D. Tepesch, G. D. Garbulsky, and G. Ceder, Phys. Rev. Lett. **74**, 2272 (1995).
[48] H. G. Scott, Acta Crystallogr., Sect. B: Struct. Crystallogr. Cryst. Chem. **B33**, 281 (1977).
[49] S. P. Ray, V. S. Stubican, and D. E. Cox, Mater. Res. Bull. **15**, 1419 (1980).
[50] L. G. Ferreira, S.-H. Wei, and A. Zunger, Int. J. Supercomput. Appl. **5**, 34 (1991).
[51] Y. Yourdshahyan, C. Ruberto, M. Halvarsson, L. Bengtsson, V. Langer, and B. I. Lundqvist, J. Am. Ceram. Soc. **82**, 1365 (1999).
[52] H. J. Rossell, J. Solid State Chem. **19**, 103 (1976).
[53] M. R. Thornber and D. J. M. Bevan, J. Solid State Chem. **1**, 536 (1970).
[54] F. Fan *et al.* [Isv. Akad. Nauk. SSSR Ser. Fiz., 114 (1962); 601 (1963)] claims to have produced a pyrochlore $Zr_2Y_2O_7$ ($x=0.33$) phase, but subsequent investigations by D. K. Smith [J. Am. Ceram. Soc. **49**, 625 (1966)], W. W. Barker [Izv. Akad. Nauk SSSR, Neorg. Mater. **8**, 2057 (1972)], and S. P. Ray and V. S. Stubican [Mater. Res. Bull. **12**, 549 (1977)] failed to produce this compound. Our results, showing a high-energy pyrochlore structure, support the notion that the reported existence of the pyrochlore structure is spurious.
[55] C. Wolverton, V. Ozoliņš, and A. Zunger, J. Phys.: Condens. Matter **12**, 2749 (2000).
[56] M. Weller, in *Proceedings of the 17th Risø International Symposium on Materials Science: High Temperature Electrochemistry: Ceramics and Metals*, edited by F. W. Poulsen, N. Bonanos, S. Linderoth, M. Morgensen, and B. Zachau-Christiansen (Risø National Laboratory, Roskilde, Denmark, 1996).
[57] A. Bogicevic and C. Wolverton (unpublished).
[58] C. Wolverton and A. Zunger, Phys. Rev. B **57**, 2242 (1998).
[59] D. W. Strickler and W. G. Carlson, J. Am. Ceram. Soc. **48**, 286 (1965).
[60] All values for ionic radii quoted in this work are Pauling radii, taken from the excellent web-based source ''WebElements'' by M. J. Winter (http://www.webelements.com).
[61] *Phase Diagrams for Zirconium and Zirconia Systems*, edited by H. M. Ondik and H. F. McMurdie (The American Ceramic Society, Westerville, OH, 1998).
[62] A. P. Sellars and B. C. H. Steele, Mater. Sci. Forum **34-36**, 255 (1988).
[63] L. J. Gauckler and K. Sasaki, Solid State Ionics **75**, 203 (1995).
[64] Y. Ohya, M. Murayama, and Y. Takahashi, Key Eng. Mater. **169-170**, 175 (1999).
[65] H. Jónsson, G. Mills, and K. W. Jacobsen, in *Classical and Quantum Dynamics in Condensed Phase Simulations*, edited by B. J. Berne, G. Cicotti, and D. F. Coker (World Scientific, Singapore, 1998).
[66] A. Bogicevic, J. Strömquist, and B. I. Lundqvist, Phys. Rev. Lett. **81**, 637 (1998); A. Bogicevic, S. Ovesson, B. I. Lundqvist, H. Brune, and D. R. Jennison, *ibid.* **85**, 1910 (2000).
[67] F. H. van Heuveln and H. J. M. Bouwmeester, J. Electrochem. Soc. **144**, 134 (1997).
[68] E. Perry Murray, T. Tsai, and S. A. Barnett, Nature (London) **400**, 649 (1999).
[69] R. J. Ackermann, E. G. Rauh, and C. A. Alexander, High. Temp. Sci. **7**, 305 (1975).